From single-molecule magnetism to long-range ferromagnetism in $Hpyr[Fe_{17}O_{16}(OH)_{12}(py)_{12}Br_4]Br_4$

C. Vecchini,[1,2] D. H. Ryan,[3] L. M. D. Cranswick,[4] M. Evangelisti,[1] W. Kockelmann,[5] P. G. Radaelli,[5] A. Candini,[1] M. Affronte,[1,2] I. A. Gass,[6] E. K. Brechin,[6] and O. Moze[2,*]

[1]*CNR-INFM S3 National Research Center, Modena 41100, Italy*

[2]*Dipartimento di Fisica, Università di Modena e Reggio Emilia, Modena 41100, Italy*

[3]*Physics Department, McGill University, Montreal, Canada H3A 2T8*

[4]*Canadian Neutron Beam Centre, NRCC, Chalk River Laboratories, Chalk River, Canada K0J 1J0*

[5]*ISIS, Rutherford Appleton Laboratory, Didcot OX11 0QX, United Kingdom*

[6]*School of Chemistry, The University of Edinburgh, Edinburgh EH93JJ, United Kingdom*

(Received 5 March 2008; revised manuscript received 6 May 2008; published 2 June 2008)

The molecular magnet $Hpyr[Fe_{17}O_{16}(OH)_{12}(py)_{12}Br_4]Br_4$ ("Fe_{17}") has a well-defined cluster spin ground state of $S=35/2$ at low temperatures and an axial molecular anisotropy of only $D\simeq -0.02$ K. Dipolar interactions between the molecular spins induce long-range magnetic order below 1.1 K. We report here the magnetic structure of Fe_{17}, as determined by unpolarized neutron diffraction experiments performed on a polycrystalline sample of deuterated Fe_{17} in zero applied magnetic field. In addition, we report bulk susceptibility, magnetization, and specific heat data. The temperature dependence of the long-range magnetic order has been tracked and is well accounted for within mean-field theory. Ferromagnetic order along the crystallographic *c* axis of the molecular spins, as determined by the neutron diffraction experiments, is in agreement with ground-state dipolar energy calculations.

DOI: 10.1103/PhysRevB.77.224403 PACS number(s): 75.50.Xx, 75.25.+z, 75.40.Cx

I. INTRODUCTION

High-spin molecular compounds are crystalline aggregates of single-domain magnetic particles, for which the intramolecular coupling is such that each molecule carries a net magnetic moment (or "molecular spin") at sufficiently low temperatures.[1–3] A uniaxial molecular anisotropy due to the crystal field generated by the surrounding organic ligands may also be present and lead to a spin ground state that is parallel to the anisotropy axis. Molecular magnets are in many ways superior to similar sized magnetic particles as, by their nature, they exhibit ideal monodispersity in size, volume, shape, and charge. Furthermore, they are soluble in common solvents and their highly modular character opens up avenues for fine tuning of their magnetic properties. In addition, molecular magnets are of interest for possible technological applications, i.e., as bits for small magnetic memory units and qubits in quantum computing[4] or as magnetic refrigerants for their enhanced magnetocaloric effect.[5]

The intramolecular and intermolecular engineering of molecular magnets can lead to the observation of long-range magnetic ordering (LRMO). The large molecular spins in these crystals take the place of the individual magnetic ions in conventional materials. The intermolecular magnetic coupling results from either *purely dipolar*[6–9] or mixed dipolar and/or weak superexchange[5,10–13] interactions. The former are, in principle, much simpler to understand because magnetic phase transitions driven solely by long-range dipolar interactions can be predicted without involving any adjustable parameters.[8,14–18] Unfortunately, very few examples of purely dipolar LRMO are known to date, and hence the investigation of magnetic phase transitions induced by dipolar interactions presents a most pertinent field of research in molecular nanomagnets.

A requirement for the experimental observation of LRMO is that the molecules should possess a large net spin ground state *S* to lead to accessible ordering temperatures. Indeed, the larger the spin, the stronger the intermolecular magnetic interaction is, likely yielding higher transition temperatures. However, *S* is also related to the anisotropy barrier given by $U=-DS_z^2(+D/4)$ for (half-) integer spin, where *D* is the axial molecular anisotropy. If the anisotropy is strong enough, then this energy barrier dominates the low-temperature behavior. The magnetic relaxation slows down notably inducing the molecular spins to freeze at temperatures much higher than the LRMO. The most obvious way to obtain a dipolarly ordered nanomagnet is thus to look for a high-spin molecule with a sufficiently low magnetic anisotropy. The latter condition is met by synthesizing molecular magnets of high symmetries and/or containing isotropic ions. The control of intramolecular interactions is indeed one of the main issues that has stimulated the research in molecular magnetism.

Using neutron diffraction to characterize magnetic order in molecular compounds is made difficult by two features of these materials: (i) they typically contain large numbers of hydrogen atoms, which leads to a substantial incoherent background; (ii) the very large number of nonmagnetic atoms in the molecules means that the nuclear scattering is far stronger than any potential magnetic signal. The first problem is readily avoided by using deuterated reagents, however, the second problem is intrinsic. In spite of this, some notable achievements have been reported. For example, single-crystal neutron diffraction was used to probe and characterize the LRMO in the organic molecular magnet *p*-NPNN,[19] in which the ordered moment is highly delocalized. The propagation vector of the *zero-field* ordered magnetic structure (which can be observed unambiguously via neutron diffraction) was determined, as was the temperature

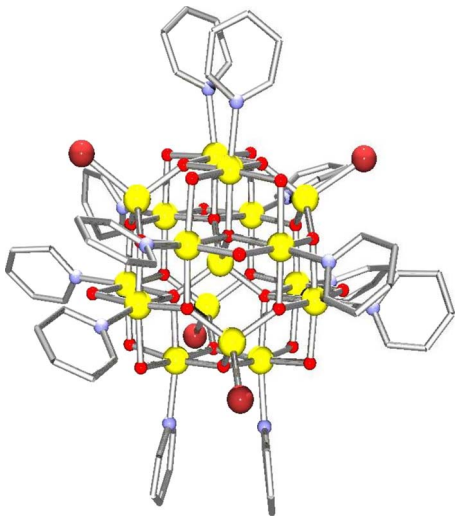

FIG. 1. (Color online) Structure of Fe_{17} (space group $R\bar{3}$, $a=b=16.1170(9)$ Å, $c=69.928(6)$ Å, hexagonal setting). The molecule contains 17 magnetically coupled Fe^{3+} atoms. Within the cluster core: brighter (yellow), darker (dark red), and smaller (red) balls represent Fe, Br, and O, respectively. CCDC-612322 contains the supplementary crystallographic data and can be obtained free of charge via the Cambridge Crystallographic Data Centre (www.ccdc.cam.ac.uk/conts/retrieving.html).

dependence of the ordered magnetic moment below $T_C \sim 0.7$ K. The experiment confirmed the ferromagnetic nature of the ordering as well as the moment direction (along the *a* axis of the orthorhombic cell). More recent neutron diffraction investigations of novel high-spin molecular nanomagnets include Mn_{10},[20] Mn_{12},[21] and Fe_8.[22] These studies, which were preceded by an unpolarized neutron diffraction investigation of polycrystalline Mn_{12} (Ref. 23) and a characterization of the ground-state static spin correlations,[24] were devoted exclusively to the *internal* magnetic structure of each cluster and confirmed the much more localized nature of the spin density for these molecular magnets. The presence of long-range ferromagnetic order in the prototypical molecular magnet Mn_{12} was recently confirmed by single-crystal neutron diffraction.[13]

The molecular magnet $Hpyr[Fe_{17}O_{16}(OH)_{12}(py)_{12}Br_4]Br_4$,[25,26] hereafter called "Fe_{17}," contains 17 Fe^{3+} ($S=5/2$) atoms per molecule, linked via oxygen atoms. The spin ground-state amounts to the truly remarkable value of $S=35/2$. The structure of the Fe_{17} molecule is shown in Fig. 1. The occurrence of such a large spin ground state is due to the presence of the competing antiferromagnetic (AF) interactions between the Fe^{3+} ions occupying the tetrahedral (T) and octahedral (O) sites. The Fe-O-Fe bridges that connect the five tetrahedral Fe^{3+} ions (one central, and four capping) to the shell of 12 octahedral Fe^{3+} ions are in the $125°-130°$ range, whereas the angles in the Fe-O-Fe bridges *between* the octahedral Fe^{3+} ions are in the $97°-101°$ range. Assuming that the larger angles promote stronger antiferromagnetic interactions, we expect the *T-O* interactions to be stronger than the *O-O* interactions, so that the 12 octahedrally coordinated Fe^{3+} ions form a ferromagnetic shell that is antiferromagnetically coupled to both the central Fe^{3+} ion and the outer four capping Fe^{3+} ions, leading to a *ferrimagnetic* molecule.[25,26]

TABLE I. Site symmetry and coordinates of the Fe^{3+} atoms in the Fe_{17} molecule.

Fe atom	Wyckoff site	x	y	z
Fe_1	6*c*	1/3	2/3	0.92
Fe_2	18*f*	0.658	0.221	0.041
Fe_3	18*f*	0.469	0.355	0.074
Fe_4	18*f*	0.455	0.239	0.108
Fe_5	18*f*	0.579	0.455	0.109
Fe_6	18*f*	0.455	0.141	0.067
Fe_7	6*c*	1/3	2/3	0.131

The Fe_{17} molecules are bound together in the crystal solely by van der Waals forces, hence prohibiting any intermolecular superexchange pathway. An interesting and possibly unique characteristic of Fe_{17} is that once the constituent ligands have been chosen, the molecules can be arranged in different crystal packings without affecting the individual molecules themselves,[9] keeping the surrounding ligands, the molecular high-spin ground state, and the magnetic anisotropy unaltered. In other words, the dipolar coupling between the molecules may be tuned with respect to single-molecular properties. The resulting interplay gives rise to behaviors ranging from superparamagnetic blocking to long-range magnetic order.[9] The present work focuses on the pyridine (pyr) derivative of the Fe_{17} molecule based on Br^- counterions, which adopts the $R\bar{3}$ space group. This system is characterized by a uniaxial anisotropy of only $D \simeq -0.02$ K, in addition to the $S=35/2$ giant-spin ground state. This combination of high spin and low anisotropy makes Fe_{17} an ideal candidate for investigating dipolar-induced long-range magnetic order. In what follows, we shall present the magnetic structure of Fe_{17} as induced by dipolar interactions solely and determined by means of neutron powder diffraction measurements. These are also accompanied by bulk magnetization, susceptibility, and magnetic field-dependent specific heat data measurements, as well as numerical simulations of the ground-state energy.

II. SAMPLE PREPARATION

The Fe_{17} molecules were obtained by dissolving $FeBr_3$ in a mixture of pyr and tetrahydrofuran. Crystallization (in the space group $R\bar{3}$) was obtained from a slow evaporation of the filtered solution after a stirring period of approximately 1 h.

The resulting cluster has at its core a central tetrahedral Fe^{3+} ion linked by O bridges to 12 outer octahedral Fe^{3+} ions, which form a truncated tetrahedron: the octagonal faces of this tetrahedron are linked by other oxygen ligands. The inner Fe^{3+} ion and the four outer Fe^{3+} sit in the tetrahedral sites of the lattice with the others occupying the octahedral sites.[25,26] Displayed in Table I are the unit cell coordinates of the seven crystallographically distinct Fe atoms which are related by symmetry operations to make up the Fe_{17} mol-

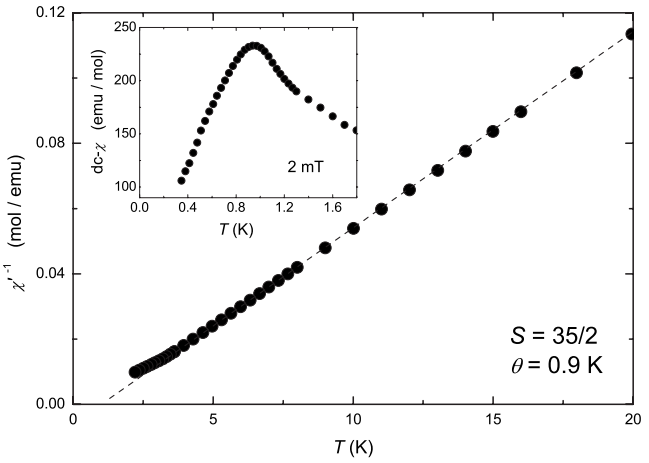

FIG. 2. Inverse of the in-phase component of the ac magnetic susceptibility collected for $f=1730$ Hz together with the fit to the Curie–Weiss law (dashed line). Inset: low temperature behavior of the susceptibility collected using a Hall microprobe with an applied field of $B_0=2$ mT.

ecule as well as the unit cell itself. Each molecule consists of 1 Fe_1, 3 Fe_2, 3 Fe_3, 3 Fe_4, 3 Fe_5, 3 Fe_6, and 1 Fe_7 atoms. The spin distribution within the cluster is thus Fe_2, Fe_3, Fe_4, and Fe_5 with *spin up* and Fe_1, Fe_6, and Fe_7 with *spin down*. This gives a net spin ground state of $S=35/2$ per molecule. Magnetization measurements on nondeuterated Fe_{17} (Refs. 25 and 26) confirm this extraordinarily high-spin ground state.

For the neutron diffraction experiments, deuteration of the sample was necessary in order to avoid the enormous incoherent scattering from hydrogen ($\sigma_{inc}=80.3$ barns). This scattering leads to an unacceptably high background signal that dominates even the coherent nuclear scattering and makes it essentially impossible to observe any magnetic scattering. The incoherent background can be reduced to an acceptable level by partial replacement of hydrogen atoms by deuterium, for which $\sigma_{inc}=2.1$ barns. The degree of deuteration of the Fe_{17} sample under investigation is estimated at approximately 80%–90%.

III. RESULTS AND DISCUSSION

Measurements of the magnetization down to 2 K and specific heat down to ≈0.3 K on powder samples were carried out in a $0<B_0<7$ T magnetic field range. Magnetization, susceptibility, and relaxation measurements below 2 K were performed using home-made Hall microprobes. In this case, the grainlike samples consisted of collections of small crystallites of about 10^{-3} mm^3. For measurements performed on powder samples, the fits were obtained taking into account random spin orientations.

A. Magnetization and susceptibility

Figure 2 shows the low-temperature behavior of the magnetic susceptibility. For the 5 K$\lesssim T\lesssim$100 K temperature range, the fit to the Curie–Weiss law $\chi=C/(T-\theta)$ provides $C=175.4$ emu K/mol and $\theta=0.9$ K. The Curie constant C equals, within the error, the expected value of a (superparamagnet) paramagnet with spin $S=35/2$ and $g=2.06$. The positive value of θ suggests predominantly ferromagnetic interactions between the $S=35/2$ magnetic units. Demagnetization effects are taken into account in the above fit by correcting the susceptibility to $\chi=\chi'/(1-\rho N\chi')$, where $\rho=3.32$ g/cm^3 is the density of the Fe_{17} complex and $N=4\pi/3$ is the demagnetizing factor of the grainlike sample approximated to a sphere. Extending the susceptibility measurements well below 2 K with our Hall microprobes reveals a prominent feature at about $T_C\approx 1$ K. Given the consistency with θ estimated from susceptibility, and anticipating the results inferred from heat capacity and neutron diffraction experiments, we associate this anomaly with a phase transition to a ferromagnetically ordered state.

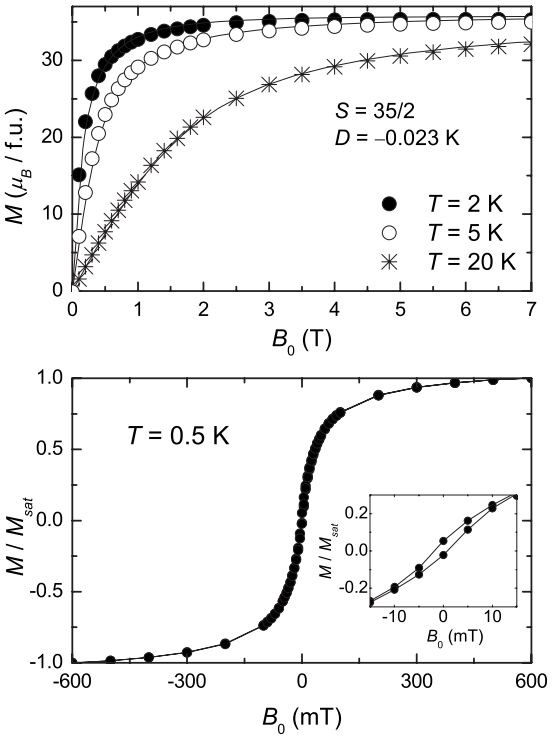

FIG. 3. Top: isothermal molecular magnetization collected at $T=2$, 5, and 20 K. Full lines represent the fit results (see text), yielding a net molecular spin $S=35/2$ and an axial anisotropy $D=-0.02$ K. Bottom: hysteresis loop measured at $T=0.5$ K with a magnification of the lowest applied-field range (inset).

Our analysis of the susceptibility is corroborated by the field dependence of the magnetization $M(B)$, as depicted in Fig. 3. The $M(B)$ curves collected for $T=2$, 5, and 20 K can be well fitted using a net molecular spin of $S=35/2$, $g=2.06$, and zero-field splitting of only $D=-0.02$ K. Although smaller trigonal components could be present, the data do not justify a more sophisticated fitting. On basis of the estimated D, the activation energy of Fe_{17} amounts to $D(S^2-1/4)\simeq 7$ K, i.e., nearly 1/9 of that in Mn_{12} acetate.[27] Accordingly, superparamagnetic blocking might be expected to occur at $T_B(Mn_{12})/9\approx 0.5$ K if intermolecular interactions were absent.[9] Assuming that the phase transition to LRMO occurs at $T_C\approx 1$ K (inset of Fig. 2), we collected a hysteresis loop in the ordered phase at $T=0.5$ K (inset of Fig. 3). We observe that Fe_{17} appears to behave like a soft

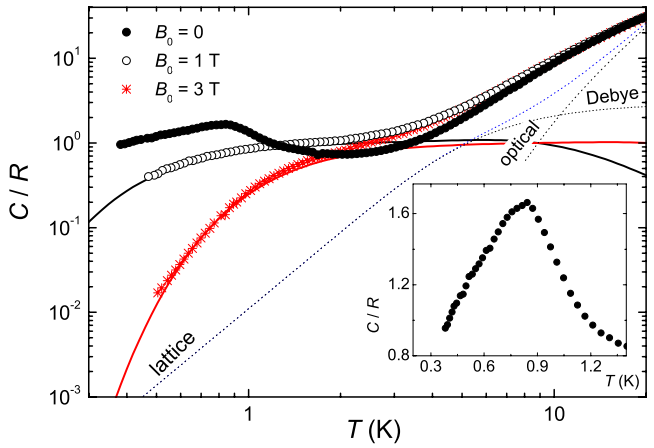

FIG. 4. (Color online) Temperature and magnetic field dependence of the specific heat C. The Schottky (solid curves) and lattice (dotted curves) contributions are explained in the text. Inset: magnification of the low-T and/or zero-field range showing the magnetic ordering.

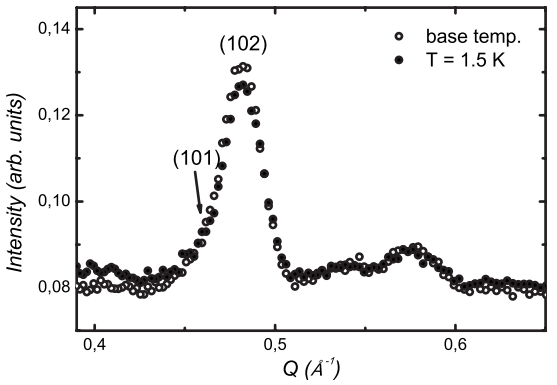

FIG. 5. Section at low values of the scattering vector Q of the time-of-flight neutron powder diffraction patterns collected on the GEM diffractometer at 1.5 K and the base temperature of the system.

ferromagnet with a small coercivity of ~2 mT. From the estimate, $D=-0.02$ K, the anisotropy likely causes a pinning of the domain wall motions leading to the slow decrease in the experimental susceptibility below T_C (Fig. 2).

B. Specific heat

Figure 4 shows the specific heat $C(T,B)$ as a function of temperature for applied fields of $B_0=0$, 1, and 3 T. In zero field, there is a prominent λ-type anomaly that develops below ~1.2 K and reaches a maximum at ~0.85 K, revealing the onset of a phase transition.[28] The magnetic nature of this event is confirmed by its disappearance upon application of a magnetic field. It is clear that the λ-type anomaly sits on top of a much broader feature, which shifts with increasing applied field toward higher temperatures. Because of the small anisotropy ($D\simeq-0.02$ K), it is expected that the magnetic contribution to $C(T,B)$ for $B_0\geq 1$ T is mainly due to a Schottky-type Zeeman splitting of the otherwise nearly degenerate spin states. Indeed, the calculated Schottky curves (solid lines in Fig. 4) arising from the field-split levels account very well for the experimental data. The lattice contributions (dashed lines in Fig. 4) were modeled as a sum of a Debye term for the acoustic low-energy phonon modes plus an Einstein term that likely arises from intramolecular vibrational modes. The fit yields $\theta_D\simeq 27$ K and $\theta_E\simeq 42$ K for the Debye and Einstein temperatures, respectively. Finally, we estimate the magnetic entropy change ΔS_m using $\Delta S_m/R=\int_0^\infty C_m(T)/(RT)\mathrm{d}T$, where $C_m(T)$ is the magnetic contribution obtained from $C(T)$ after subtracting the lattice contribution. We find $\Delta S_m=3.7R$, in good agreement with the entropy expected $R\ln(2S+1)\simeq 3.6R$, given $S=35/2$. As already anticipated, we can therefore safely attribute the λ feature to a phase transition of the Fe_{17} molecular spins.

C. Neutron diffraction

Two sets of neutron diffraction measurements were performed. The first set was performed on the GEM time-of-flight diffractometer, located at the ISIS pulsed neutron source, Rutherford Appleton Laboratory, U.K. A sample weighing approximately 2 g was inserted in a 6 mm diameter vanadium sample can with a copper "cold finger" inserted from top to bottom for the length of the sample can in order to assist in the thermalization of the sample.

An "orange-type" cryostat and a ^{3}He closed cycle system were used to cool the sample, and measurements were performed at four different temperatures: the ambient (293 K), an intermediate temperature (50 K), the low T (~1.5 K), and the base temperature of the ^{3}He cryostat. Data were normalized to the wavelength distribution of the incident neutron beam. The most important part of the data is contained in the low-angle banks, which corresponds to the small values of the scattering vector Q, where one can expect magnetic scattering.

No changes were observed in the scattering patterns between 293 and 1.5 K, confirming that the high-spin system remains paramagnetic, with no long-range magnetic order, down to at least 1.5 K. This is consistent with the bulk data, reported above, which indicate that magnetic correlations are not expected to set in above $T\approx 1.2$ K. The unchanging nuclear scattering also shows that the material retains its $R\bar{3}$ crystal symmetry on cooling. The first indication of magnetic ordering comes from a suppression of the paramagnetic background scattering for $Q<0.45$ Å^{-1} on cooling below 1.5 K, as seen in Fig. 5. This is typical of a transition from a disordered to an ordered state. The observed Bragg intensities are dominated by the nuclear scattering and any magnetic scattering is expected to be weak. In spite of this limitation, a discernible increase in intensity was noted on cooling from 1.5 K, particularly for $Q\sim 0.48$ Å^{-1}, which corresponds to the overlapping nuclear (101) and (102) reflections (Fig. 5). This increase in intensity with decreasing temperature is positive confirmation of the presence of magnetic Bragg scattering. Furthermore, as no new reflections were observed, the scattering from the magnetic structure is superimposed on the nuclear scattering, and the ordering wave vector $\mathbf{k}$ of the magnetic structure is therefore {000}. This corresponds to either a commensurate ferromagnetic or commensurate antiferromagnetic structure. The peak shape is

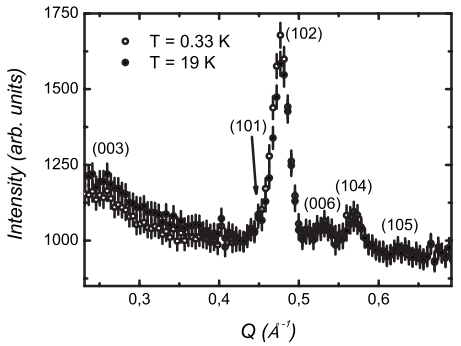

FIG. 6. Section at low-scattering vectors of the neutron powder diffraction patterns collected on the DUALSPEC spectrometer at $T=0.33$ and 19 K. Note the loss of paramagnetic scattering for $Q \leq 0.45$ Å^{-1} and the extra intensity at the (102) and (104) positions.

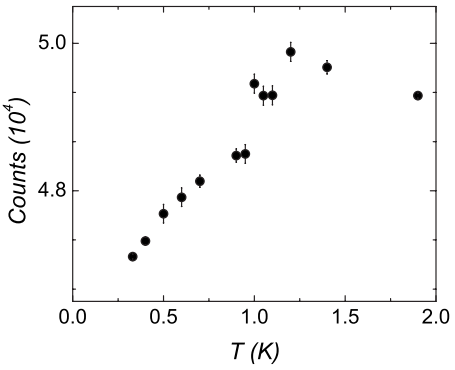

FIG. 7. Integrated intensity for 0.2 Å$^{-1} \leq Q \leq 0.35$ Å^{-1} showing the marked reduction in paramagnetic scattering on cooling through T_C.

of the expected double-exponential pseudo-Voigt type, commonly obtained on time-of-flight diffraction instruments, so that the ordering can be taken to be three-dimensional in nature.

The second set of neutron diffraction measurements consisted of a more complete and detailed temperature dependent survey of the magnetic signal and was performed on the constant wavelength C2 DualSpec spectrometer (located at the Canadian Neutron Beam Centre, Chalk River, Canada) on the same sample of deuterated Fe_{17}. An incident neutron wavelength of 2.3723 Å was used and a modified Oxford Instruments Heliox ^{3}He cold stage was adapted to fit into an orange cryostat that was mounted on the spectrometer. This system enabled subkelvin temperatures down to 330 mK to be reached with typical holding times of ~48 h. Earlier experience. with mounting powdered samples on this Heliox system showed that cooling time constants of several days can be observed unless significant efforts are taken to ensure thermalization.[29] The following procedure, which has been found to yield thermalization times of less than 30 s, was therefore used. The 1.17 g of powder Fe_{17} was mixed with 1.25 g of 99.99% pure copper powder and hydraulically pressed into a 6 mm inside diameter oxygen-free, high-conductivity copper can to form a 26 mm long solid rod inside the can. While this packing does not affect the properties of the Fe_{17}, it does add some fcc-Cu reflections, however, the first of these occur at $Q \sim 3$ Å^{-1}, well outside our region of interest. Diffraction patterns were collected at temperatures from 0.33 to 1.4 K to follow the magnetic ordering in detail. In addition, a nonmagnetic reference pattern was taken at 19 K.

Two signatures of magnetic ordering are clearly visible in Fig. 6 which shows a comparison of the 19 and 0.33 K diffraction patterns: (i) The background scattering for $Q \leq 0.45$ Å^{-1} is significantly lower, reflecting that the loss of the paramagnetic contribution as a long-ranged magnetic order is established, and (ii) extra intensity is evident at the (102) and (104) reciprocal lattice positions, reflecting the presence of magnetic order.

Figure 7 shows that the temperature dependence of the low-angle background can be used to obtain a preliminary estimate for T_C. There is a striking drop below ~1 K as long-ranged magnetic order develops and the incoherent paramagnetic scattering is reduced. This observation is inconsistent with random spin freezing, such as superparamagnetic blocking, and requires that the magnetic transition at T_C to be a long-ranged ordered state. No new reflections are observed in Fig. 6, and the weak magnetic scattering is superimposed on much stronger nuclear reflections. Both the (102) and (104) reflection intensities increase on cooling, while the (006) and much weaker (003) reflections show no temperature dependence. The fundamental selection rule for magnetic neutron diffraction is that the neutrons are scattered by the components of the magnetic moment *perpendicular* to the scattering vector; the systematic absence of magnetic peaks of the type (00l) is direct evidence that the ordered magnetic moment lies along the c axis (the moment direction with respect to the uniaxial direction can be specified even for powder samples, as is the case here).[30] Fits to the *line shape* show no temperature dependence associated with the onset of magnetic order, indicating that the magnetic peaks have the same width as the underlying nuclear reflections and that the magnetic and crystallographic structures have the same correlation lengths. This supports our conclusion that the ordering at T_C is long ranged in nature.

The only constraints imposed on the magnetic structure are that all single-ion Fe^{3+} spins in the molecule are *nonzero* and equal in magnitude to $S=5/2$ and that each molecule consists of a well-defined *colinear ferrimagnetic* arrangement of spins. The present neutron data are restricted to a limited range of scattering vector. This implies that a traditional Rietveld refinement of the crystal and magnetic structures is not feasible. With the available neutron data and the above constraints, we have utilized the theory of irreducible representations[31,32] for magnetic groups to define a magnetic structure compatible with the neutron and bulk macroscopic magnetic data. This theory is particularly valid for second order phase transitions. There are six possible irreducible representations of the space group $R\bar{3}$ for $\mathbf{k}=\{000\}$. For the two types of magnetic sites, 6c and 18f, which comprise the Fe_{17} molecule, *each* of these six representations occur for *both* sites. The basis vectors of these representations for each of the magnetic sites were calculated using SARA h-representational analysis[33] (downloadable at ftp://ftp.ill.fr/pub/dif/sarah/). The selected basis vectors belong to two of the six irreducible presentations, Γ_1 and Γ_2, which corre-

TABLE II. Basis vectors and basis vector components (m_x, m_y, m_z) of the irreducible group representations for the space group $R\bar{3}$ with propagation vector $\mathbf{k}=\{000\}$. The atom notations $6c_1$ and $6c_2$ refer to atom 1 and its symmetry equivalent atom 2 in an *adjacent* molecule.

Irreducible representation	Basis vector	$6c$	$18f$
Γ_1	ψ_1	$(6c_1)$ $00+m_z$	$(18f_1)$ $00+m_z$
		$(6c_2)$ $00+m_z$	$(18f_2)$ $00+m_z$
			$(18f_3)$ $00+m_z$
			$(18f_4)$ $00+m_z$
			$(18f_5)$ $00+m_z$
			$(18f_6)$ $00+m_z$
Γ_2	ψ_2	$(6c_1)$ $00+m_z$	$(18f_1)$ $00+m_z$
		$(6c_2)$ $00-m_z$	$(18f_2)$ $00+m_z$
			$(18f_3)$ $00+m_z$
			$(18f_4)$ $00-m_z$
			$(18f_5)$ $00-m_z$
			$(18f_6)$ $00-m_z$

spond to the magnetic structures with all moments aligned either parallel or antiparallel to the c axis, respectively. The other four, Γ_3, Γ_4, Γ_5, and Γ_6, represent various planar configurations. We can discard these latter configurations on the basis of the observed intensities, which clearly point to an axial configuration. Furthermore, some of the basis vectors for Γ_3, Γ_4, Γ_5, and Γ_6 give sites where a magnetic moment is not allowed. Table II lists the irreducible representations and their corresponding basis vectors for the magnetic structures compatible with our data. Figure 8 displays our simulations of the expected powder diffraction patterns for the two corresponding magnetic structures Γ_1 and Γ_2.

The ferromagnetic configuration Γ_1 attributes a small intensity to the (101) reflection and a larger assignment of intensity to the (102) reflection. This is in stark contrast to the antiferromagnetic configuration Γ_2, for which the intensity ratios of these two peaks are practically inverted. The representations corresponding to the four planar configurations all give intensity at the (003) position. Of the six possible models, only the axial ferromagnet is in accord with our data. We therefore conclude that dipolar interactions do, in fact, favor this configuration. As a further confirmation and anticipating Sec. IV, dipolar calculations indicate indeed that of the two ground states displayed in Fig. 9, the axial ferromagnet has a lower energy than the axial antiferromagnet.

The Fe-O cluster forming the core of the Fe_{17} molecule behaves as a single, exchange-coupled $S=35/2$ entity. The temperature dependence of the ordered magnetization below T_C reflects excitations of these giant-spin orderings in the mean field established by intercluster dipolar forces and manifests itself in the intensity of the (102) reflection. This peak intensity is directly proportional to the square of the ordered moment (Fig. 10). Fitting the observed magnetic intensity to a $S=35/2$ Brillouin function, neglecting any effects due to the small anisotropy, yields an ordering temperature of 1.13(2) K in good agreement with values obtained

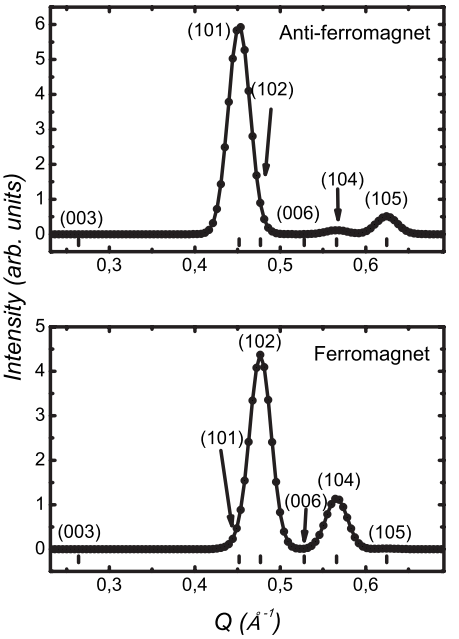

FIG. 8. Simulations of the low-Q magnetic diffraction pattern at $T=0.33$ K for an antiferromagnetic (AF) (top) and ferromagnetic (FE) (bottom) alignment of Fe_{17} molecules along the c axis.

from both susceptibility and heat capacity measurements. We emphasize here that the neutron diffraction data do more than simply confirm the transition temperature; they unequivocally demonstrate that the magnetic order is long ranged and ferromagnetic in nature, with moments aligned parallel to the c axis.

IV. GROUND-STATE ENERGY CALCULATIONS

We calculated ground-state dipolar energies E_{dip} for the pointlike Heisenberg spins arranged in crystallographic lattice analogs to that of Fe_{17}. In particular, the position of the spins was fixed accordingly to molecular centroids. The mo-

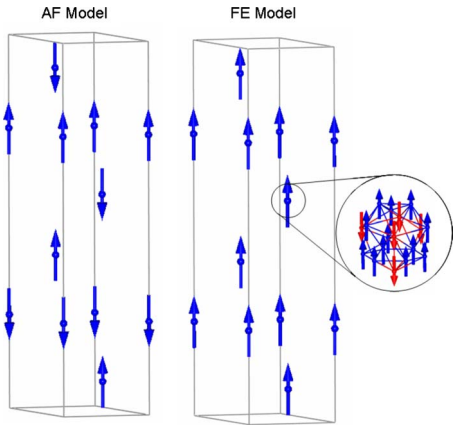

FIG. 9. (Color online). Representation of the axial AF and axial FE structures, as induced by dipolar interactions between the Fe_{17} molecules, indicated by large arrows (blue). Inset: ferrimagnetic structure of the Fe_{17} molecule represented by 12 *up spins* (blue) and 5 *down spins* (red)

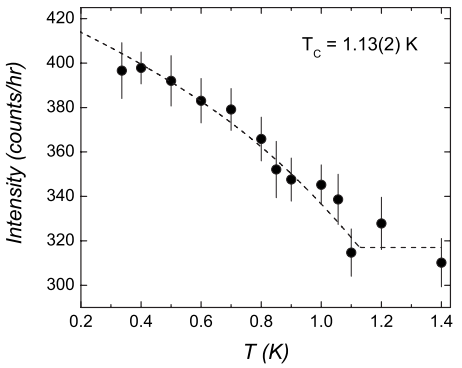

FIG. 10. Temperature dependence of (102) peak intensity showing the onset of magnetic order below $T_C=1.13(2)$ K. The underlying nuclear intensity was taken from data recorded at 19 K, while the magnetic intensity was fitted to $S=35/2$ mean-field behavior (dotted line; see text).

lecular symmetry of Fe_{17} is such that the centroid of each individual molecule corresponds to the position of the Fe^{3+} ion at the center of the molecule. The net spin carried by each molecule is represented by a vector $\vec{S}$ of length $S=35/2$. This classical approximation is good because of the large value of the spin. Therefore, the molecular magnetic moment is $\vec{\mu}=\mu_B\vec{g}\cdot\vec{S}$. For the sake of simplicity, we assume the isotropic $\vec{g}$ with $g=2$.

If the magnetic cell contains m spins, the magnetic structure is given by a set of m magnetic moment vectors $\vec{\mu}_i$. The dipolar energy per ion of an ordered crystal is given by

$$E_{\text{dip}}=\frac{R}{2mk_B}\sum_{i=1}^{m}\vec{\mu}_i\cdot\vec{H}_i,$$

where $\vec{H}_i$ is the molecular field at site i, given by

$$\vec{H}_i=-\sum_{j\neq i}^{N}\left\{\frac{\vec{\mu}_j}{r_{ij}^3}-3\frac{(\vec{\mu}_i\cdot\vec{r}_{ij})\vec{r}_{ij}}{r_{ij}^5}\right\}.$$

We evaluate these summations using free boundary conditions for spherical shaped systems, for which all spins inside the sphere are allowed to interact. Slow numerical convergences are usually solved by the summation techniques such as the Ewald method. However, we checked that direct sums for a cutoff radius larger than 200 Å (corresponding roughly to 280 00 spins) provide reproducible E_{dip} results with differences within 2%.

The calculations are carried out for the spin configurations depicted in Fig. 9, i.e., the ferroelectric (FE) and AF spin alignments along the c axis. We obtain $E_{\text{dip}}=0.2$ and 2.0 K for FE and AF, respectively. Since they differ by 1 order of magnitude, we can clearly conclude that the most probable configuration is ferromagnetic, corroborating the neutron diffraction analysis.

V. CONCLUSIONS

The Fe_{17} magnetic molecule represents a unique system, in which neutron scattering techniques can be successfully employed to assess the long-range ferromagnetically ordered structure induced by dipolar interactions.[9] A highly symmetric molecular core and a correspondingly small uniaxial anisotropy combine to support the occurrence of magnetic ordering at accessible temperatures. Neutron diffraction measurements performed on powder samples of Fe_{17} confirm the type of the order and the direction of the ordered magnetic moments with respect to the crystallographic unit cell. A small but clear magnetic signal is observed and successfully tracked in the temperature interval $0.33\ \text{K}\leq T\leq 1.4$ K. The transition temperature $T_C=1.13(2)$ K is in good agreement with susceptibility and specific heat data. Furthermore, unlike most other examples of long-range ordered molecular magnets, it is possible to obtain the relatively large amounts of deuterated Fe_{17} essential for a successful neutron diffraction experiment. Modeling the magnetic structure with a net spin $S=35/2$ positioned in the molecular centroids shows a good agreement with the experimental data, indicating that the Fe_{17} molecule behaves as an atom with a macrospin given by the sum of the contribution of the constituent Fe^{3+} ions. This encouraging result should stimulate neutron powder diffraction experiments in other molecular superparamagnets where long-range order may be active.

ACKNOWLEDGMENTS

O.M. and D.H.R. acknowledge many useful discussions with J. M. Cadogan (University of Manitoba). The dedicated assistance of the CNBC staff was essential to the success of the neutron diffraction work. E.K.B. thanks the EPSRC-GB and Leverhulme Trust (U.K.). Financial support from NSERC (DHR and the CNBC) and FQRNT (DHR) is gratefully acknowledged. This work was partially supported by MAGMANet (Grant No. NMP3-CT-2005-515767).

*Author to whom correspondence should be addressed. Also at Dipartimento di Fisica, Università di Modena e Reggio Emilia, Modena 41100, Italy; oscar.moze@unimore.it

[1] D. Gatteschi and R. Sessoli, Angew. Chem., Int. Ed. **42**, 268 (2003).

[2] S. J. Blundell and F. L. Pratt, J. Phys.: Condens. Matter **16**, R771 (2004).

[3] B. Barbara, C. R. Phys. **6**, 934 (2005).

[4] M. Affronte *et al.*, J. Phys. D **40**, 2999 (2007).

[5] M. Evangelisti, A. Candini, A. Ghirri, M. Affronte, E. K. Brechin, and E. J. L. McInnes, Appl. Phys. Lett. **87**, 072504 (2005).

[6] A. Bino, D. C. Johnston, D. P. Goshorn, T. R. Halbert, and E. I. Stiefel, Science **241**, 1479 (1988).

[7] A. Morello, F. L. Mettes, F. Luis, J. F. Fernández, J. Krzystek, G. Aromí, G. Christou, and L. J. de Jongh, Phys. Rev. Lett. **90**, 017206 (2003).
[8] A. Morello, F. L. Mettes, O. N. Bakharev, H. B. Brom, L. J. de Jongh, F. Luis, J. F. Fernández, and G. Aromí, Phys. Rev. B **73**, 134406 (2006).
[9] M. Evangelisti *et al.*, Phys. Rev. Lett. **97**, 167202 (2006).
[10] M. Affronte, J. C. Lasjaunias, W. Wernsdorfer, R. Sessoli, D. Gatteschi, S. L. Heath, A. Fort, and A. Rettori, Phys. Rev. B **66**, 064408 (2002).
[11] A. Yamaguchi *et al.*, J. Phys. Soc. Jpn. **71**, 414 (2002).
[12] M. Evangelisti, F. Luis, F. L. Mettes, N. Aliaga, G. Aromí, J. J. Alonso, G. Christou, and L. J. de Jongh, Phys. Rev. Lett. **93**, 117202 (2004).
[13] F. Luis, J. Campo, J. Gómez, G. J. McIntyre, J. Luzón, and D. Ruiz-Molina, Phys. Rev. Lett. **95**, 227202 (2005).
[14] P. Panissod and M. Drillon, in *Magnetism: Molecules to Materials IV*, edited by J. S. Miller and M. Drillon (Wiley-VCH, Weinheim, Germany, 2002), Chap. 7.
[15] J. F. Fernández and J. J. Alonso, Phys. Rev. B **62**, 53 (2000).
[16] J. F. Fernández, Phys. Rev. B **66**, 064423 (2002).
[17] X. Martínez-Hidalgo, E. M. Chudnovsky, and A. Aharony, Europhys. Lett. **55**, 273 (2001).
[18] M. Evangelisti, F. Luis, F. L. Mettes, R. Sessoli, and L. J. de Jongh, Phys. Rev. Lett. **95**, 227206 (2005).
[19] A. Zheludev, E. Ressouche, J. Schweizer, P. Turek, M. Wan, and H. Wang, Solid State Commun. **90**, 233 (1994).
[20] A. Caneschi, D. Gatteschi, R. Sessoli, and J. Schweizer, Physica B (Amsterdam) **241-243**, 600 (1998).
[21] R. A. Robinson, P. J. Brown, D. N. Argyriou, D. N. Hendrickson, and S. M. J. Aubin, J. Phys.: Condens. Matter **12**, 2805 (2000).
[22] Y. Pontillon, A. Caneschi, D. Gatteschi, R. Sessoli, E. Ressouche, J. Schweizer, and E. Lelieve-Berna, J. Am. Chem. Soc. **121**, 5342 (1999).
[23] P. A. Reynolds, E. P. Gilbert, and B. N. Figgis, Inorg. Chem. **35**, 545 (1996).
[24] M. Hennion, L. Pardi, I. Mirebeau, E. Suard, R. Sessoli, and A. Caneschi, Phys. Rev. B **56**, 8819 (1997).
[25] G. W. Powell, H. N. Lancashire, E. K. Brechin, D. Collison, S. L. Heath, T. Mallah, and W. Wernsdofer, Angew. Chem., Int. Ed. **43**, 5772 (2004).
[26] I. A. Gass, C. J. Milios, M. Evangelisti, S. L. Heath, D. Collison, S. Parsons, and E. K. Brechin, Polyhedron **26**, 1835 (2007).
[27] A. C. R. Sessoli, D. Gatteschi, and M. A. Novak, Nature (London) **365**, 141 (1993).
[28] M. Evangelisti, F. Luis, L. J. de Jong, and M. Affronte, J. Mater. Chem. **16**, 2534 (2006).
[29] I. A. Swainson and D. H. Ryan (private communication 2007).
[30] G. Shirane, Acta Crystallogr. **12**, 282 (1959).
[31] E. F. Bertaut, J. Appl. Phys. **33**, 1138 (1962).
[32] E. F. Bertaut, in *Treatise on Magnetism*, edited by G. T. Rado and H. Suhl (Academic, New York, 1963), Vol. III, p. 149.
[33] A. S. Wills, Physica B (Amsterdam) **276-278**, 680 (2000).